F_O-F_1 coupling and symmetry mismatch in ATP synthase resolved in every F_O rotation step

Shintaroh Kubo[1,2,*], Toru Niina[1], & Shoji Takada[1,*]

[1] Department of Biophysics, Graduate School of Science, Kyoto University, Kyoto 606-8502, Japan

[2] Department of Anatomy and Cell Biology, McGill University, Montréal, Québec H3A 0C7, Canada

* Corresponding author:

Shintaroh Kubo, Department of Anatomy and Cell Biology, McGill University, Montréal, Québec H3A 0C7, Canada. e-mail: shintaroh.kubo@mail.mcgill.ca

Shoji Takada, Department of Biophysics, Graduate School of Science, Kyoto University, Kyoto 606-8502, Japan e-mail: takada@biophys.kyoto-u.ac.jp

Abstract

The F_OF_1 ATP synthase, essential for cellular energy production, is composed of the F_O and F_1 rotary motors. While both F_O and F_1 have pseudo-symmetric structures, their symmetries do not match. How the symmetry mismatch is solved remains elusive due to missing intermediate structures of rotational steps. Here, for ATP synthases with 3- and 10-fold symmetries in F_1 and F_O, respectively, we uncovered the mechanical couplings between F_O and F_1 at every 36º rotation step via molecular dynamics simulations and comparison of cryo-electron microscopy structures from three species. We found that the frustration is shared by several elements. The F_1 stator partially rotates relative to the F_O stator via elastic distortion of the b-subunits. The rotor can be distorted. The c-ring rotary angles can be deviated from symmetric ones. Additionally, the F_1 motor may take non-canonical structures relieving stronger frustration. Together, we provide comprehensive understanding to solve the symmetry mismatch.

Key words: F_OF_1 ATP synthase, Molecular motor, Molecular dynamics simulation

Introduction

Adenosine triphosphate (ATP) is mainly synthesized by the enzyme F_OF_1 ATP synthase[1–3]. The enzyme is composed of two rotary motors, the F_O and F_1 motor, and these motors are connected by two stalks, a central rotor and a peripheral stalk (Fig. 1a). The membrane-embedded F_O motor rotation driven by the proton motive force causes the central rotor rotation. The latter induces a series of conformational changes in the F_1 motor, where ATP is synthesized from adenosine diphosphate (ADP) and inorganic phosphate (Pi). The F_OF_1 ATP synthase is also known as a reversible machine, which can hydrolyze ATP to pump protons against the proton motive force.

The F_1 motor contains the central rotor (γ/ε-subunit in bacterial F_1) and an $\alpha_3\beta_3$ hexamer made of three αβ dimers (Fig. 1a). Each αβ dimer has catalytic sites for the ATP synthesis reaction and take three distinct chemical states and conformations[4], which are conventionally denoted as the ATP-bound state (TP for brevity), the ADP-bound state (DP), and the empty state (E). Especially, the β-subunit takes markedly different conformations among the three states; for the case of the *Bacillus* PS3 ATP synthase, which will be our target in this study, its C-terminal segment takes a “closed” conformation in the TP state, while it takes an "open" conformation in the DP and the E states[5]. Since a single-molecule measurement showed that the F_1 motor in the ATP hydrolysis mode uncovered 120º-stepwise rotation of the central rotor, accompanied by progress of the chemical states in $\alpha_3\beta_3$[6]. Thus, coupled with the nucleotide-dependent conformational change in the α/β-subunits, one round of the F_1 motor results in the hydrolysis or synthesis of three ATP molecules, depending on the central rotor direction. The F_O motor is made of an a-subunit and a c-ring, which is a ring-shaped c-subunit oligomer working as a rotor (Fig. 1a). The number of c-subunits in the c-ring varies between 8-17 depending on the species[7–13]; 10 subunits in the *Bacillus* PS3 ATP synthase. Each c-subunit has one key proton-relaying residue. Single-molecule experiments for *Escherichia coli* ATP synthase (10 subunits) identified 36º stepwise c-ring rotations[14]. Thus, one round of the F_O motor was driven by the transfer of the same number of protons as that of c-subunits.

In contrast to the mechanisms of each motor, the mechanism of the coupling between the F_O and F_1 motors is less clear. Because the number of c-subunits in the c-ring is not a multiple of three in

most cases, the mean number of protons necessary for the synthesis of one ATP is not an integer value, which is sometimes called a symmetry mismatch. There has been much debate regarding the mechanism by which F_OF_1 ATP synthase resolves this mismatch[15]. For *Bacillus* PS3 ATP synthases, the two motors are connected via a central rotor made of $c_{10}\gamma\varepsilon$ and a peripheral stalk made of $b_2\delta$ (Fig. 1a). Some early studies suggested the elastic distortion of the central rotor, γ-subunit[16–18]. Other studies have anticipated the role of δ[19]. Recent cryo-EM structures of mitochondria and *Bacillus* PS3 ATP synthases point to distortion in b-subunits[5,20]. From recent cryo-EM studies, the symmetric mismatch and the relatively rigid rotor together imply that the $\alpha_3\beta_3$ hexamer rotate relative to the a-subunit[19,21]. Sobti *et al*. resolved three different rotational states and one sub-state in *E. coli* ATP synthase. The sub-state structure essentially had the same F_1 configuration as one of the three state structures, but the c_{10}-ring together with the F_1 stator, $c_{10}\alpha_3\beta_3\gamma\varepsilon$, rotated relative to the F_O stator. Comparing individual conformations, we see that the b-subunits have significantly different conformations. Therefore, the existence of the sub-state and the flexibility of the b-subunit may be necessary for resolving the symmetry mismatch. Notably, however, the cryo-EM models in Sobti *et al*. include structural models for four c_{10}-ring rotation states out of ten possible rotational states. Perhaps other states are more fragile and/or more short-lived, so that high-resolution models could not be built. Moreover, cryo-EM models provide static snapshots, as usual; for example, how the sub-state arises, how the b-subunit distortion resolves the mismatch, and when and how the F_1-motor undergoes structural changes in response to the c-ring rotation remain unclear.

In this study, to address the F_O-F_1 coupling and the molecular mechanisms to solve the symmetry mismatch, we performed molecular dynamics (MD) simulations that mimic the ATP synthesis dynamics for one round of rotation in the holo-complex of the *Bacillus* F_OF_1 ATP synthesis. While many molecular simulations have been reported so far for each of the F_O and F_1 motors[18,22–28], to the best of our knowledge, this study provides MD simulations for the first time for one round of ATP synthase holo-complex. Our dynamic simulations showed the order and timing of the structural changes in the three $\alpha\beta$-pairs in the F_1 motor during ten 36º-rotation steps of the F_O motor. Furthermore, relaxation simulations with a fixed c-ring rotation angle in every 36º-step exhibited the c-ring-dependent partial rotation of the F_1 stator relative to the F_O stator and some twists in the rotor.

Then, motivated by the simulation results, we conducted a comparative analysis of cryo-EM structures from three species, accounting for the structural changes in the ATP synthases. Together, we reveal how to solve the symmetry mismatch in F_OF_1 ATP synthesis in unprecedented detail.

Results and Discussion

Simulating the rotation dynamics in the ATP synthase holo-complex

The *Bacillus* PS3 ATP synthase cryo-EM study provides holo-complex structure models in the three rotational states: A (PDB ID: 6N2Y, Fig. 1a left), B (PDB ID: 6N2Z), and C (PDB ID: 6N30)[5]. In all of these holo-complex models, F_1 was in the catalytic dwell. We introduce the numbering of the three αβ pairs, αβ1, αβ2, and αβ3, counterclockwise starting from the α/β-subunits furthest from the b-subunit (Fig. 1a, middle). In the A state, αβ1, αβ2, and αβ3 are in the E, TP, and DP states, respectively. The structural change from A to B (the AB process) involves the counterclockwise rotation of c_{10}-ring by 3×36º, together with the progress of the chemical steps in the three αβ pairs; αβ1, αβ2, and αβ3 change to the DP, E, and TP states, respectively. Similarly, the transitions from B to C (the BC process) and from C to A (the CA process) involve rotations by four and three 36º c-ring rotation steps, respectively, coupled with the chemical state changes in αβ pairs. We call this whole process the 3-4-3 pathway, assuming that the entire process starts and ends in the A state.

Given the 3-4-3 pathway in the three cryo-EM rotational states, we envisioned to simulate the process that the F_1 motor in the A state would reach the B state when the F_O c_{10}-ring rotates counterclockwise by 3×36º. To simulate the conformational change in the AB process, we need to model in a way that each αβ pair can accommodate both A and B state conformations. For this purpose, we employed a double-basin model that encodes A and B state conformations separately for each αβ system (see Methods for details). The double-basin model concisely builds two distinct conformational basins controlling both the energy barrier in between and the relative stabilities of the two basins[29–31] (Fig. 1b). Also, for the BC and CA processes, introducing the double-basin models that

connect the B and C states and that connect the C and A states, we expected to observe the respective state transitions in the F_1 motor while the c_{10}-ring rotates 4×36º and 3×36º degrees, respectively (Fig. 1c). To ensure the energetics of the ATP synthesis process, we set the summation of the relative stabilities of the three αβ double-basin models in the AB, BC, and CA processes to ~ +36 kcal, which approximates the free energy increase for the synthesis of 3 ATP molecules from ADP and Pi.

In the simulations, we rotated the c_{10}-ring by 36° with a constant angular velocity over 10^6 MD steps, followed by a c_{10}-ring pause for 9×10^6 MD steps. Note that 10^4 MD steps were denoted as one frame. For each case, we repeated the same simulations ten times with different stochastic forces. The structural transitions in each αβ are monitored by its reaction coordinate χ, which takes negative and positive values when αβ is in the pre- and post- states in the double-basin system, respectively. For the AB process, we repeated this rotation step four times (the upper c-ring panel of Fig. 2ab). For the BC and CA processes, we began with 10×10^6 MD equilibration steps in the initial c_{10}-ring angle and then repeated the rotation step four times (the upper c-ring panel of Fig. 2cd and Fig.2e, respectively).

How many F_O c-ring rotation steps are necessary to induce the F_1 nucleotide state transition?

We monitored the structural changes in each αβ (Fig. 2, χ pre → post) as well as other structures. When all three χ's in F_1 changed from negative to positive values, we regarded F_1 to have completed its transition. Fig. 2a shows a representative trajectory of the AB process: (1) The αβ1 started transitions from the E state to the DP state at the ~100th frame immediately after the c-ring rotated 36°, followed by rapid transitions back and forth. (2) The αβ3 made a transition from the DP to the TP state at the ~2200th frame when the c-ring completed the third 36°rotation. (3) Finally, αβ2 transited from the TP to the E state at the ~2500th frame, corresponding to the dissociation of a synthesized ATP molecule. At this stage, all three αβ pairs completed their transitions (blue triangle in the figure). This was within the third rotation step. Thus, in this trajectory, three c-ring rotation steps induced a complete structural transition in F_1 during the AB process. Of the ten repeated trajectories, six showed

similar results; three c-ring rotation steps induced complete F_1 transitions. In the two trajectories, four c-ring rotation steps were necessary to induce F_1 transitions (one case depicted in Fig. 2b). The remaining two did not complete the F_1 transition at the end of the simulations (Supplementary Fig. 1a). Thus, as expected from the cryo-EM structures, we observed that in the majority of cases, the F_1 structural transitions in the AB process were completed with the three 36°-c-ring-rotation steps.

Next, we describe the BC process. For this process, we first took the 3000th frame snapshot in the representative trajectory of the AB process (shown in Fig. 2a) as the initial structure. Fig. 2c shows the typical trajectory of the BC process. In this trajectory, the αβ1 and αβ2 pairs exhibited unstable fluctuations until αβ3 transitioned from the TP to the E state at the ~4200th frame. Once αβ3 is in the E state, both αβ1 and αβ2 are stabilized in the TP and DP states. The overall structural change in F_1 was completed after the fourth c_{10}-ring rotation step. All trajectories which complete conformational changes (four out of ten) were completed with four c-ring 36°-rotation steps (Supplementary Fig. 1b). Therefore, we conclude that four 36°-rotation steps are necessary to induce complete structural changes in F_1 in the BC process with this initial structure. We mentioned about the BC process on the 4-3-3 pathway in Supplementary Text 1.

Finally, the CA process is simulated. First, we started the simulation with the 5000th frame snapshot of the representative BC process trajectory in the 3-4-3 pathway. Fig. 2e shows a typical trajectory (Supplementary Fig 1d). Initially, αβ3 gradually changed from the E to the DP state between the 200th and 900th frames. Then, αβ1 made the transitions from the TP to the E state and settled down in the E state at the ~ 3100th frame right when the third c-ring rotation step in the CA process was over. This is quickly followed by the transition in αβ2 from the DP to the TP state around the 3300th frame when the overall conformational change in this process was over. The F_1 transition was completed within the third 36°-c-ring-rotation step in six of the ten trajectories tested. The F_1 transition was completed within the second and fourth 36°-rotation steps, each in one trajectory. The remaining two trajectories did not exhibit complete structural changes. Therefore, the dominant pathway in the CA process completes the F_1 state transitions by the three c-ring rotation steps. We mentioned about the CA process on the 4-3-3 pathway in Supplementary Text 1 and Fig. 2bd.

Altogether, our simulation predominantly showed the 3-4-3 pathway, which is in harmony with the cryo-EM studies. Additionally, we noticed a common feature as suggested in a classic work[1,32]: Of the three F_1 αβ structure transitions in each process, the αβ that changes from the TP to the E state is a bottleneck that tends to decide the number of necessary 36°-rotation steps. ATP synthesis in this enzyme has the rate-limiting process of the product dissociation.

Partial rotation of the F_1 stator accompanied by the b-subunits bending

Recent cryo-EM studies by Murphy *et al.*[19] and Sobti *et al.*[21] reported more than three rotational states for ATP synthases from *Polytomella* sp. and *E. coli*, respectively, both of which contain a c_{10}-ring. In both cases, they found varying degrees of rotation of the F_1 stator relative to the F_O stator, raising the possibility of a partial rotation of the F_1 stator as a mean to solve the symmetry mismatch. However, these structural models contain only a limited c-ring rotation step. How was the symmetry mismatch solved in every 36º-rotation step? To address this point, we calculated the rotary angle θ of the F_1 stator relative to the F_O stator during the trajectories (Fig. 3a-e); here, the F_1 stator and the F_O stator mean F_1 $\alpha_3\beta_3$ and F_O a-subunit, respectively. For this purpose, we fixed the rotation axis of the F_O c_{10}-ring to the z-axis and F_O a-subunit to the positive x-axis and monitored the rotary angle θ of F_1 $\alpha_3\beta_3$ around the z-axis (further details in the Methods). Fig. 3a-e plot the time courses of θ for the same five trajectories as in Fig. 2a-e.

First, we examined the F_1 stator angle θ of the AB process (Fig. 3ab). The F_1 stator started to rotate ~20° counterclockwise dragged by the $c_{10}\gamma\varepsilon$ rotation. In addition, the γ-subunit is distorted ~-10° (the fourth panel of Fig. 3a). When the c-ring rotates counterclockwise, the rotation up to 10º tends to be absorbed by the distortion of the γ-subunit. In the subsequence process within the AB process in the 3-4-3 pathway (Fig. 3a), the F_1 stator tends to return to the initial angle. Importantly, the return of the F_1 stator angle occurred together with the structural transition in F_1. Once F_1 adopts

conformations compatible with the cryo-EM structure of the B state, the F_1 stator can accommodate the angle θ~0 (Fig. 3f, left).

Next, we analyzed the simulation trajectories of the BC process in the 3-4-3 pathway (Fig. 3c). When the c_{10}-ring started to rotate at the 1000th frame (the fourth cumulative c-ring rotation step is denoted as $n = 4$), the F_1 stator is dragged by the rotor rotation, similarly to the above case ($n = 1$). At the 1000th frame, while the c_{10}-ring rotated by 36°, the F_1 stator rotated by ~20°. However, in sharp contrast to the above AB process, the F_1 stator angle never returned to the initial angle (~0°) until the simulation ended ($n = 5 - 7$) (Fig. 3f, right). At the end (the 5000th frame), the F_1 stator was rotated by ~20°. At this stage, the accumulated rotation in the c_{10}-ring was 7×36°, counting from the A state, whereas the F_1 motor made two progressive transitions rotating the chemical states by $2 \times 120°$. The difference in the rotation angle, $7 \times 36°$-$2 \times 120°$=12°, may be adsorbed by the counterclockwise rotation of the F_1 stator.

Notably, the rotation of the F_1 stator in the BC process is accompanied by a large distortion of the b-subunit (the right-end extrusion in Fig. 3f right), in which a part that is close to F_1 is rotated counterclockwise, whereas a part of the b-subunit bound to the F_O a-subunit remains in the original position. The distortion of the b-subunit is a passive conformational change. Owing to this distortion, elastic energy is charged into the b-subunit. We propose that the presence of the b-subunit, in addition to the balance of rotation angles discussed later, is the reason why the BC process requires more c-subunits rotation than other processes (Supplementary Text 2). To quantify the motion of the b-subunit, we performed principal component analysis (PCA) on the b-subunit; the first principal component (PC1) in the AB process represents a counterclockwise tilt along the F_1 stator (Fig. 3g, left). The time course of the PC1 value (the third panel in Fig. 3a) indicates that it changes closely in parallel with the F_1 stator angle θ. Note that a positive PC1 indicates a counterclockwise distortion of the b-subunit (the direction of the arrow in Fig. 3g).

Third, we examined the CA process of the 3-4-3 pathway. As shown in Fig. 3e panel, we observed a clockwise rotation of the F_1 stator back to the initial angle. The b-subunit also followed clockwise tilting back to the relaxed structure in the A state (third panel in Fig. 3e). Therefore, it can

be said that the CA process resolves the distortion caused by the counterclockwise rotation accumulated in the AB and BC processes. Lastly, we also mentioned the rotation of F_1 stator for the 4-3-3 pathway in Supplementary Text 1.

Relaxation simulations with the fixed c_{10}-ring rotary angles

While these simulations provided dynamic view to resolve the symmetry mismatch, the obtained structures are inherently transient due to a relatively fast rotation of c_{10}-ring. To obtain well-equilibrated structures at every 36º-c_{10}-ring-rotation steps, which were not seen by cryo-EM studies, we conducted further MD simulations of relaxation. We fixed the c_{10}-ring rotation step at $n \times 36$º-rotation steps for $n = 1{\sim}10$ and conducted further 2000-frame simulations ten times with the initial structure taken from the $n \times 1000$th frame snapshots in the previous trajectories.

We found a clear trend in the AB process. For $n = 1$, we started the simulations from the 1000th frame snapshot of the representative trajectory (the red curve in Fig. 4a), as well as from the trajectory in which the F_1 rotated the least amount at the 1000th frame among (the blue curve in Fig. 4a). Both sets of simulations steadily showed counterclockwise rotations of the F_1 stator with varying degrees of rotation angles up to ~30º (Fig. 4b, panel 1). Thus, our simulation models gave consistent results with recent cryo-EM studies[19]. We also monitored the distortion of rotor $c_{10}\gamma\varepsilon$ (Supplementary Fig. 3). In the $n = 2$ state, the F_1 stator was rotated ~20°, and then rotated clockwise to ~ -10° in the c-ring state $n = 3$. Although the angle of the initial structure in $n = 3$ had a much more counterclockwise rotated, we found its clockwise rotation back to ~0º during the relaxation simulation (the left-side green curve in Fig. 4a). Thus, the clockwise return of the F_1 stator at $n = 3$ is a robust process.

In the BC process, we observed similar but not identical trends. In the c_{10}-ring state $n = 4$, the F_1 stator rotated counterclockwise by ~20º, which is very similar to the c_{10}-ring state $n = 1$. This angle was maintained in the c-ring states $n = 5$ and 6. Particularly, in the $n = 6$ state, we also observed marked, albeit incomplete, structural transitions in the F_1 motor. Supplementary Fig. 4

shows that αβ3 exhibited irreversible and bottleneck transitions from the TP to E states in four of the ten trajectories. In the c-ring state $n = 7$, which is the final state in the BC process, the F_1 stator is slightly, but not completely, turned to reach ~+10°. A simple estimation may help our understanding: the c-ring rotated by 7×36º from the A state, while the F_1 motor rotated by 2×120º. The difference was 12º.

Finally, in the CA process, we found the result to be somewhat similar to that of the AB process (Fig. 4d 8-10). In the c_{10}-ring state $n = 8$, the F_1 stator rotated counterclockwise by ~30º, similar to the c_{10}-ring state $n = 1$. We found that the rotor was significantly distorted at $n = 8$, which is different from the $n = 1$ case. The F_1 stator slightly rotated back but remained rotated at ~10° in the c-ring state $n = 9$. Finally, after the full round, the F_1 stator settled down at the original 0º-angle. To check if the settled down was robustness, we simulated from another initial state in which the F_1 stator rotated 20º (the right-side green curve in Fig. 4a). As we expected, we found the same settled down, therefore, we conclude that the F_1 stator settles down to ~0º when the system is fully relaxed after one round of the c_{10}-ring.

In summary, we see that the F_1 stator constantly rotates back and forth, dragged by the c_{10}-ring rotation and by the chemical state change in F_1, but eventually returns to its initial position after the full round. We have discussed the angle change from a typical trajectory, and in the next section, we will discuss it using more statistical values.

On the symmetry mismatch between F_O and F_1

The stepwise rotations of the F_O c_{10}-ring and F_1 motor shown in Fig. 5a (upper panel) illustrate the symmetry mismatch. By symmetry, the ideal elementary rotation steps of the c_{10}-ring and F_1 motor were 36º and 120º, respectively. We assume that the c_{10}-ring and the F_1 motor rotation steps coincided at the ground state angle, the A state, chosen as the angle 0º (this is an approximation, but it turned out reasonable). Then, the 120º-step of the F_1 motor was flanked by 3×36 º =108º and 4×36 º =144º of the c_{10}-ring steps with 108º-step closer. It is reasonable to assume that a smaller deviation in the angle corresponds to a lower energy of frustration. Thus, the 3×36 º =108º step of the c_{10}-ring may be

realized to accommodate the F_1 motor 120º-state. In the same way, the 240º-step of the F_1 motor was flanked by 6×36 º =216º and 7×36 º =252º of the c_{10}-ring steps with 252º-step closer. Obviously, the 360º-step was realized both by the c-ring and the F_1 motor without frustration, which led to the 3-4-3 pathway, consistent with all three cryo-EM studies. This minimal-deviation-rule directly provides the simplest reasoning for the 3-4-3 pathway. The same rule may be applicable to c-rings composed of subunits other than ten (Fig. 5b). The c_8-ring, the c_9-ring, and the c_{11}-ring may exhibit the 3-2-3, 3-3-3, and 4-3-4 pathways starting from the ground state.

The next question is how to resolve the mismatch between the F_O c_{10}-ring and the F_1 motor in the primary rotation states B ($n = 3$) and C ($n = 7$) in the 3-4-3 pathway, namely the difference between 120º and 108º in the B state and the difference between 240º and 252º in the C state. Structures provided by Guo *et al.* suggested that the mismatch of the range ~12º can mostly be compensated by the rotation of the F_1 stator via the distortion of the b-subunit (Table 1, Fig. 5c, and Supplementary Text 3).

The mismatch between the F_O c_{10}-ring and the F_1 motor increases after the 36º c-ring rotation from the primary states A, B, and C, namely the rotation states $n = 1, 4,$ and 8. This range of mismatches cannot be absorbed by the F_1 stator rotation. Instead, it is realized by the combinations of the three types of elastic structural changes in the structures of Sobti *et al.* and Murphy *et al.* (Fig. 5c and Supplementary Text 3): a) the b-subunits accommodate $\pm(7 - 14)^{\circ}$, which appears as the rotation of the F_1 stator, b) the c_{10}-ring rotation deviates $\pm(11 - 13)^{\circ}$ from the ideal angles, and c) the rotor distortion is in the range of $\pm(4 - 11)^{\circ}$. In contrast, the F_1 motor showed a fluctuation of only $\sim \pm 2^{\circ}$. It is a key feature that the F_1 motor maintains the canonical angle with slight fluctuations in all cryo-EM structures. The corresponding angles monitored in our MD simulations are consistent with these experiments (Fig. 5a, the second and third panels), except that the MD simulations assumed uniform 36º-rotation steps of the c_{10}-ring, which is not rigorously the case in cryo-EM structures.

In all the AB, BC, and CA processes, the first 36º-c-ring-rotation step from the primary rotation states induces the counterclockwise rotation of the F_1 stator ($n = 1, 4, 8$). This is in agreement

with the findings of Murphy *et al.*[19]. The second 36º-c-ring-rotation step tends to keep the F_1 stator rotated, which is often accompanied by significant distortion of the rotor and incomplete transitions in the F_1 motor ($n = 2, 5, 9$). The F_1 motor may take structures different from canonical three-fold rotary states. These are strongly frustrated states and are likely too dynamic to be modeled at high resolution in cryo-EM studies. The simulations showed relatively diverse configurations. Here, we suggest an interesting scenario: In some of these states, the F_1 motor may utilize the 80º sub-step to the so-called binding-dwell. Namely, the 80º sub-step of the F_1 motor is close to 2×36º=72º step of c_{10}-ring, the 200º sub-step is close to both 5×36º=180º and 6×36º=216º of c_{10}-ring, and the 320º sub-step of the F_1 motor is close to 9×36º=324º step of c_{10}-ring, which may serve to relieve the highly frustrated energies. In the last 36º-c-ring-rotation step of the AB, BC, and CA processes, the F_1 stator finally rotates clockwise back to near the original angle ($n = 3, 7, 10$); and the final angles differ in the three processes: ~-10°, ~+10°, and ~0º for the AB, BC, and CA processes, respectively.

Conclusions

Using the recently obtained cryo-EM structures of the *Bacillus* PS3 F_OF_1 ATP synthases, we carried out MD simulations of the holo-complex that mimicked three cycles of ATP synthesis, the AB, BC, and CA processes, and one round of rotor rotation. We found that the AB, BC, and CA processes completed the respective structural changes in F_1 with the highest probabilities when the c_{10}-ring made three, four, and three 36º-rotation steps, which is consistent with the experimental results. At all ten 36º-step of c_{10}-ring rotations, we investigated the holo-complex structural changes that resolve the symmetry mismatch between F_O and F_1. The symmetry mismatch was resolved by the distortion of a few parts. First, the b-subunit distortion led to the rotation of the F_1 stator back and forth relative to the F_O stator. Second, the rotor itself is distorted to a lesser extent. Third, the comparative analysis of cryo-EM structures from the three species showed that the c-ring rotary angles can be deviated from symmetric ones. Since the movement of the β-subunit in αβ2 is suppressed by the b-subunit and ε-subunit, a stronger torque is required to overcome this barrier during the BC process. Simulation

results, together with the comparative analysis of recent cryo-EM structure models, reveal molecular reasoning to resolve the symmetry mismatch.

Since we adopted a simple approach to simulates rotary motions of the ATP synthase holo-complex, it has some limitations. First, since we used a classical MD with a coarse-grained molecular representation, the chemical reaction itself was only dealt with conformational changes correlated with chemical reactions. Second, since we adopted a predefined time course of c_{10}-ring rotation, we have not been able to reproduce the effects of stochastic proton transport. Third, since some parts of the b-subunit around δ-subunit was missing in cryo-EM models, we cannot deny the possibility that this missing region contribute to the conformational change. Despite these limitations, our MD simulations revealed the mechanical coupling between F_1 and F_O with reasonable accuracy in detail, which is sufficient to fully explain the solution of the symmetry mismatch in ATP synthases.

Materials & Methods

Model building

We used the *Bacillus* PS3 ATP synthase structure model for the A state (Protein Data Bank (PDB) ID, 6N2Y) obtained by cryo-EM as the reference structure for the corresponding A state in our MD simulations[5]. The model consists of eight proteins and 22 subunits, $ab_2c_{10}\alpha_3\beta_3\gamma\delta\varepsilon$. Based on the PDB structure, we modeled loops for the missing regions in the a-subunit using MODELLER[33]. For the sake of structural symmetry, the range of residues used for three α- and β-subunits was made the same: I8 to S501 for α-subunits and T2 to M469 for β-subunits. In addition, one of the b-subunits (called b2 in the original PDB data) contains a C-terminal region that is neither modeled nor has a sequence assigned. This region was excluded from the simulation system. We established the coordinate system such that the center of masses of the F_O c_{10}-ring was set at its original point, the rotation axis of the c_{10}-ring coincided with the z-axis, and R169 of the F_O a-subunit was on the x-axis.

We also prepared reference structure information for B and C states. Notably, we did not use the structural models given in the PDB for these states. Instead, we mostly used the structure information for the A state because we assumed that the A state was the ground-state form. In the structure-based simulation, the reference structure for each subunit was used to define the lowest energy state of the subunit, except for the structures of $\alpha_3\beta_3$. Assuming a change in the chemical state and the corresponding change in the stable conformation, we repositioned the reference structures in a rotary manner. For example, the reference structure information of αβ1 in the B state, which is in the DP state, was copied from the reference structure of αβ3 in the A state, having the same DP state. Similarly, all reference structure information could be obtained from those in the A state.

MD simulation setting

We performed coarse-grained MD simulations using the reference structure described above. In the coarse-grained representation, one amino acid was treated as one particle located at the Cα position. We primarily used the energy function AICG2+[34,35], which has been intensively used in simulations of large molecular complexes[25,36,37]. In this function, the reference structure was assumed to be the most stable conformation, and many parameters inside were determined from the atomic interactions in the all-atom reference structures (detail in Supplementary Text 4).

In this study, to investigate the mechanical coupling between F_O and F_1 parts, we designed a minimal setup that mimicked ATP synthesis reactions induced by the c-ring rotation driven by the proton-motive-force in a simple design. Assuming the c-ring rotation driven by the proton-motive force, we made the c-ring rotate with a predefined time course. In the F_1 part, for each αβ pair that sandwiches the ATP catalytic site, we set multiple basins that encode ATP-bound (TP), ADP-bound (DP), and empty (E) state conformations. When the state transition settled to the new state, we considered that the corresponding chemical event occurred (detail in Supplementary Text 5).

In our minimal design, the F_O a-subunit was a rigid part of the F_O stator and was fixed to the initial structure and position. The F_O c_{10}-ring was treated as a rigid body and rotated by design around the z-axis with a predefined schedule.

With these setups, we ran simulations on several processes: AB, BC, and CA. First, in the AB process, the simulation started from the reference structure built from PDB ID: 6N2Y. In the simulation, the c_{10}-ring rotated stepwise 36º by 36º as designed. The coupling between F_O and F_1 led the three double-basin systems of the F_1-motor to exhibit their conformations and reach the post-state (state B). Then, we selected a representative snapshot from the trajectory and treated it as the initial model for the subsequent simulation of the BC process. The simulation of the BC process began with this model. After three or four c-ring 36º-rotation steps, we also picked a representative snapshot of the initial structure of the CA process. Finally, we performed a CA simulation. In each simulation, we repeated 10 MD runs with different stochastic forces using CafeMol version 2.1[38]. Unless otherwise noted, we took 4×10^7 MD steps, 5×10^7 MD steps, and 5×10^7 MD steps for the AB, BC, and CA

processes, respectively. We used underdamped Langevin dynamics at 323 K temperature and set the friction coefficient to 2.0 (CafeMol unit); default values were used for the others.

Data Availability

The cryo-EM structures used in this paper are available download from the Protein Data Bank under PDB IDs 6N2Y, 6N2Z, and 6N30 for the *Bacillus* PS3 ATP synthase; 6WNQ, 6OQV, 6OQR, 6OQS, 6OQT, 6OQU, 6PQV, 6OQW, and 6WNR for the *E. coli* ATP synthase; 6RDH, 6RDW, 6RDZ, 6RE8, 6REB, and 6RES for the *Polytomella* sp. ATP synthase.

Code Availability

All MD simulations in this paper was performed by CafeMol software. It can be downloaded from https://www.cafemol.org.

References

1. Boyer, P. D. The ATP synthase - A splendid molecular machine. *Annu. Rev. Biochem.* **66**, 717–749 (1997).
2. Yoshida, M., Muneyuki, E. & Hisabori, T. ATP synthase - A marvellous rotary engine of the cell. *Nat. Rev. Mol. Cell Biol.* **2**, 669–677 (2001).
3. Walker, J. E. The ATP synthase: The understood, the uncertain and the unknown. *Biochem. Soc. Trans.* **41**, 1–16 (2013).
4. Abrahams, J. P., Leslie, A. G. W., Lutter, R. & Walker, J. E. Structure at 2.8 Â resolution of F1-ATPase from bovine heart mitochondria. *Nature* **370**, 621–628 (1994).
5. Guo, H., Suzuki, T. & Rubinstein, J. L. Structure of a bacterial ATP synthase. *elife* **8**, 1–17 (2019).
6. Noji, H., Yasuda, R., Yoshida, M. & Kinosita Jr., K. Direct observation of the rotation of F1-ATPase. *Nature* **386,** 299–302 (1997).
7. Watt, I. N., Runswick, M. J., Montgomery, M. G., Walker, J. E. & Leslie, A. G. W. Bioenergetic cost of making an adenosine triphosphate molecule in animal mitochondria. *Proc. Natl. Acad. Sci.* **107**, 16823–16827 (2010).
8. Stock, D., Leslie, A. G. W. & Walker, J. E. Molecular architecture of the rotary motor in ATP synthase. *Science* **286**, 1700–1705 (1999).

9. Mitome, N., Suzuki, T., Hayashi, S. & Yoshida, M. Thermophilic ATP synthase has a decamer c-ring: Indication of noninteger 10:3 H+/ATP ratio and permissive elastic coupling. *Proc. Natl. Acad. Sci.* **101**, 12159–12164 (2004).
10. Meier, T., Polzer, P., Diederichs, K., Welte, W. & Dimroth, P. Structure of the rotor ring of F-type Na+-ATPase from Ilyobacter tartaricus. *Science.* **308**, 659–662 (2005).
11. Matthies, D. *et al.* The c13 ring from a thermoalkaliphilic ATP synthase reveals an extended diameter due to a special structural region. *J. Mol. Biol.* **388**, 611–618 (2009).
12. Vollmar, M., Schlieper, D., Winn, M., Büchner, C. & Groth, G. Structure of the c14 rotor ring of the proton translocating chloroplast ATP synthase. *J. Biol. Chem.* **284**, 18228–18235 (2009).
13. Pogoryelov, D., Yildiz, Ö., Faraldo-Gómez, J. D. & Meier, T. High-resolution structure of the rotor ring of a proton-dependent ATP synthase. *Nat. Struct. Mol. Biol.* **16**, 1068–1073 (2009).
14. Düser, M. G. *et al.* 36° step size of proton-driven c-ring rotation in F o F 1-ATP synthase. *EMBO J.* **28**, 2689–2696 (2009).
15. Sielaff, H., Yanagisawa, S., Frasch, W. D., Junge, W. & Börsch, M. Structural asymmetry and kinetic limping of single rotary F-ATP synthases. *Molecules* **24**, 24–29 (2019).
16. Pänke, O. & Rumberg, B. Kinetic modeling of rotary CF0F1-ATP synthase: Storage of elastic energy during energy transduction. *Biochim. Biophys. Acta* **1412**, 118–128 (1999).
17. Cherepanov, D. A., Mulkidjanian, A. Y. & Junge, W. Transient accumulation of elastic energy in proton translocating ATP synthase. *FEBS Lett.* **449**, 1–6 (1999).
18. Okazaki, K. & Hummer, G. Elasticity, friction, and pathway of γ-subunit rotation in F o F 1 -ATP synthase. *Proc. Natl. Acad. Sci.* **112**, 10720–10725 (2015).
19. Murphy, B. J. *et al.* Rotary substates of mitochondrial ATP synthase reveal the basis of flexible F1-Fo coupling. *Science.* **364**, (2019).
20. Stewart, A. G., Lee, L. K., Donohoe, M., Chaston, J. J. & Stock, D. The dynamic stator stalk of rotary ATPases. *Nat. Commun.* **3**, (2012).
21. Sobti, M. *et al.* Cryo-EM structures provide insight into how E. coli F1Fo ATP synthase accommodates symmetry mismatch. *Nat. Commun.* **11**, (2020).
22. Mukherjee, S. & Warshel, A. Electrostatic origin of the mechanochemical rotary mechanism and the catalytic dwell of F1-ATPase. *Proc. Natl. Acad. Sci. U. S. A.* **108**, 20550–20555 (2011).
23. Bai, C., Asadi, M. & Warshel, A. The catalytic dwell in ATPases is not crucial for movement against applied torque. *Nat. Chem.* **12**, 1187–1192 (2020).
24. Pu, J. & Karplus, M. How subunit coupling produces the γ-subunit rotary motion in F 1-ATPase. *Proc. Natl. Acad. Sci. U. S. A.* **105**, 1192–1197 (2008).
25. Kubo, S., Niina, T. & Takada, S. Molecular dynamics simulation of proton-transfer coupled rotations in ATP synthase FO motor. *Sci. Rep.* **10**, 8225 (2020).
26. Pogoryelov, D. *et al.* Microscopic rotary mechanism of ion translocation in the F(o) complex of ATP synthases. *Nat. Chem. Biol.* **6**, 891–899 (2010).
27. Hayashi, S. *et al.* Molecular mechanism of ATP hydrolysis in F1-ATPase revealed by molecular simulations and single-molecule observations. *J. Am. Chem. Soc.* **134**, 8447–8454 (2012).
28. Dittrich, M., Hayashi, S. & Schulten, K. On the mechanism of ATP hydrolysis in F1-ATPase. *Biophys. J.* **85**, 2253–2266 (2003).
29. Okazaki, K., Koga, N., Takada, S., Onuchic, J. N. & Wolynes, P. G. Multiple-basin energy landscapes for large-amplitude conformational motions of proteins: Structure-based molecular dynamics simulations. *Proc. Natl. Acad. Sci. U. S. A.* **103**, 11844–11849 (2006).
30. Best, R. B., Chen, Y. G. & Hummer, G. Slow protein conformational dynamics from multiple experimental structures: The helix/sheet transition of Arc repressor. *Structure* **13**, 1755–1763 (2005).
31. Maragakis, P. & Karplus, M. Large amplitude conformational change in proteins explored with a plastic network model: Adenylate kinase. *J. Mol. Biol.* **352**, 807–822 (2005).
32. Boyer, P. D. The binding change mechanism for ATP synthase - Some probabilities and possibilities. *Biochim. Biophys. Acta* **1140**, 215–250 (1993).

33. Šali, A. & Blundell., T. L. Comparative protein modelling by satisfaction of spatial restraints. *J. Mol. Biol.* **234**, 779–815 (1993).
34. Li, W., Terakawa, T., Wang, W. & Takada, S. Energy landscape and multiroute folding of topologically complex proteins adenylate kinase and 2ouf-knot. *Proc. Natl. Acad. Sci.* **109**, 17789–17794 (2012).
35. Li, W., Wang, W. & Takada, S. Energy landscape views for interplays among folding, binding, and allostery of calmodulin domains. *Proc. Natl. Acad. Sci. U. S. A.* **111**, 10550–10555 (2014).
36. Takada, S. *et al.* Modeling structural dynamics of biomolecular complexes by coarse-grained molecular simulations. *Acc. Chem. Res.* **48**, 3026–3035 (2015).
37. Kubo, S., Li, W. & Takada, S. Allosteric conformational change cascade in cytoplasmic dynein revealed by structure-based molecular simulations. *PLoS Comput. Biol.* **13**, 8502 (2017).
38. Kenzaki, H. *et al.* CafeMol: A coarse-grained biomolecular simulator for simulating proteins at work. *J. Chem. Theory Comput.* **7**, 1979–1989 (2011).

Acknowledgements

S.K. was supported by JSPS Research Fellowship. This work was also supported by the MEXT grant JPMXP1020200101 as "Program for Promoting Researches on the Supercomputer Fugaku" (ST), partly by JSPS KAKENHI grants 20H0593 (ST) and 21H02441 (ST), and by by the Japan Science and Technology Agency (JST) grant JPMJCR1762 (ST).

Author Contributions

S.K. and S.T. conceived and designed the project; T.N. developed the simulation code; S.K. performed the simulations; S.K. and T.N. analyzed the data; S.K. assembled figures, and all authors discussed the results and were involved in the manuscript writing process.

Competing Interests statement

The authors declare no competing interests.

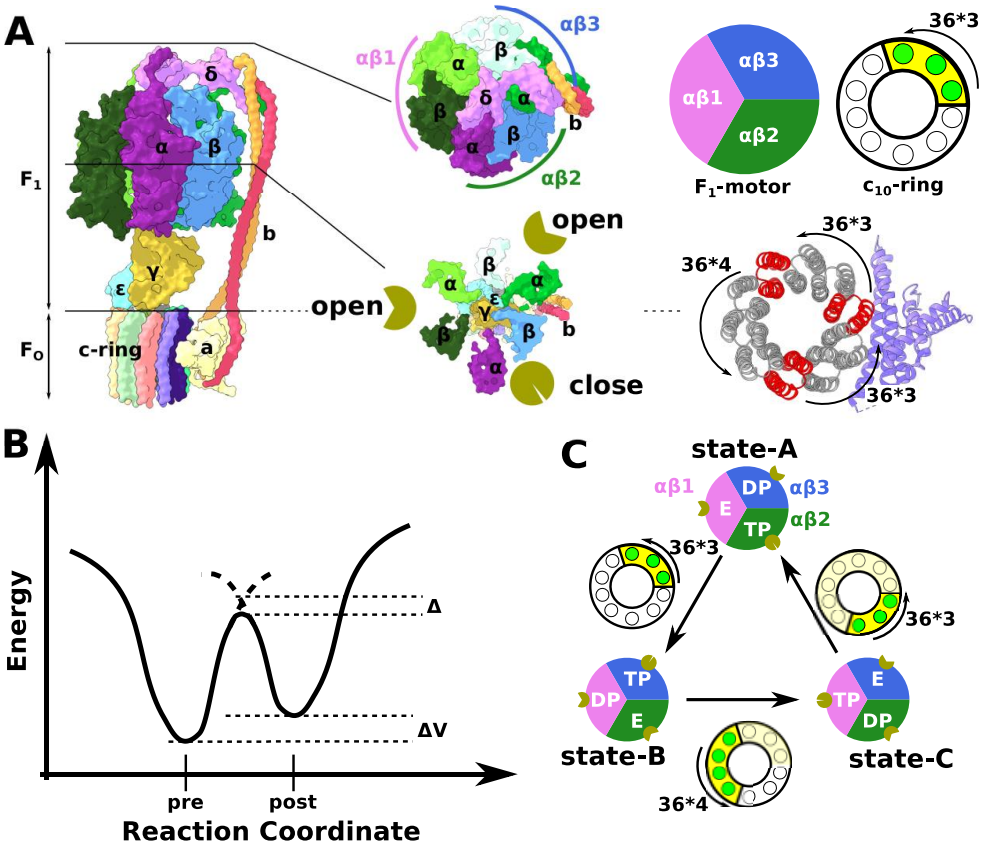

Fig. 1 Structure of F_OF_1 ATP synthase and the simulation system.

a. (Leftmost) The structure of *Bacillus* PS3 F_OF_1 ATP synthase holo-complex (the A state, PDB ID: 6N2Y). The F_1 motor (top half) contains δ: pink; $\alpha_3\beta_3$ hexamer made of three αβ pairs, αβ1: lime green and green; αβ2: violet and sky blue; αβ3: yellow green and white; γ: dark yellow; ε: cyan. The F_O motor contains c_{10}-ring: pastel-colored barrel-shaped objects; a-subunit: pale yellow; b-subunits: pale red and orange. In the 6N2Y structure, αβ1, αβ2, and αβ3 take the E, TP, and DP states, respectively, and these take the open, closed, and open structures, respectively indicated by golden pie chart pictures. (Right) Guo *et al.* built three different ATP synthase conformations: A (PDB ID: 6N2Y), B (6N2Z), and C (6N30). The structure differences from A to B (AB), B to C (BC), and C to A (CA) contain three, four, and three 36°-c_{10}-ring-positional-rotation in a counterclockwise direction, respectively. The red c-subunits indicate the ones closest to the a-subunit in the A, B, and C states. **b.** The schematic view of the double-basin model. "pre" and "post" indicate the minimum energy structures for the pre- and post-structures, respectively. Δ and ΔV are parameters to control the barrier

518 height and relative stability between two minima. **c.** The conformational change cycle in the ATP
519 synthesis mode.
520

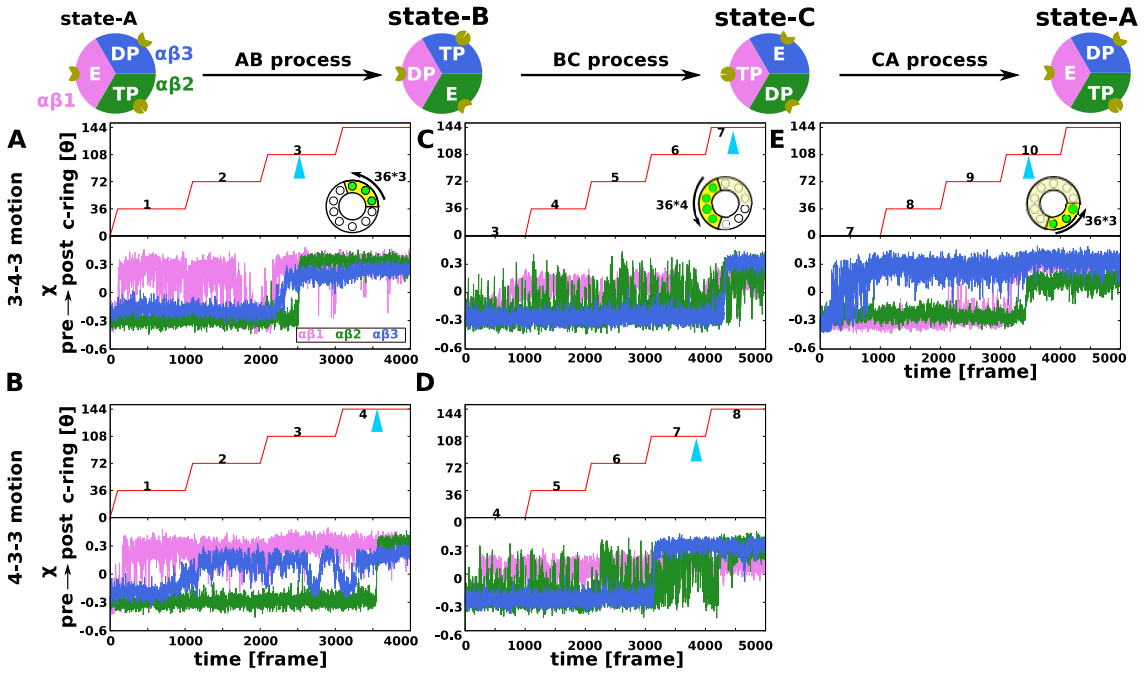

521
522 **Fig. 2 Structure change in the F_1 motor during MD simulations of one round c_{10}-ring rotations.**
523 **a-e.** Representative MD simulation trajectories for the AB (panel A), BC (panel C), and CA (panel E)
524 processes in the 3-4-3 pathway, and for the AB (panel B) and BC (panel D) processes in the 4-3-3
525 pathway. Results of all the 10 trajectories are given in Supplementary Fig. 1. Each panel shows the
526 c_{10}-ring rotation time schedule (upper) and the reaction coordinate for the structure changes: χ of the
527 αβ1, αβ2, and αβ3 (red, green, and blue, respectively) (bottom). The triangle mark colored cyan shows
528 the timing when all the three αβ's completed their structural changes. The CA process trajectories in
529 the 4-3-3 motion is shown in Supplementary Fig. 2. One frame of time corresponds to 10^4 MD steps.
530

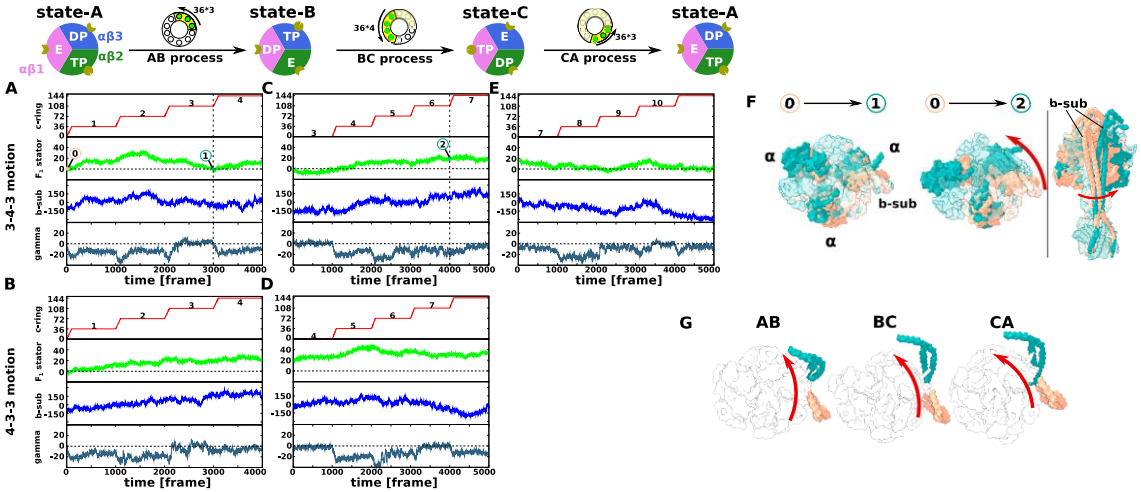

Fig. 3 F_O-F_1 coupling during MD simulations of one round c_{10}-ring rotations.

a-e. Each panel plots, from the top to bottom, the rotation angle of the c_{10}-ring, the rotation angle of the F_1 stator, the first principal component about the b-subunit motions, and the rotation angle of the rotor defined by the angle of the upper part of γ-subunit relative to the rotation angle of c_{10}-ring (the moving average over 10 frames) for the same trajectories as those shown in Fig. 2a-e. **f.** Superimposed snapshots shown in Fig. 3a-c trajectories 0, 1, and 2, respectively. The snapshot at time point 0 is colored dark salmon, and those at time point 1 and 2 are colored dark cyan. The three α-subunits are opaque to make it easier to see, and the others are translucent. **g.** The direction of structural change of the first principal component in the principal component analysis for the b-subunit. The first principal component value increases from dark salmon to dark cyan.

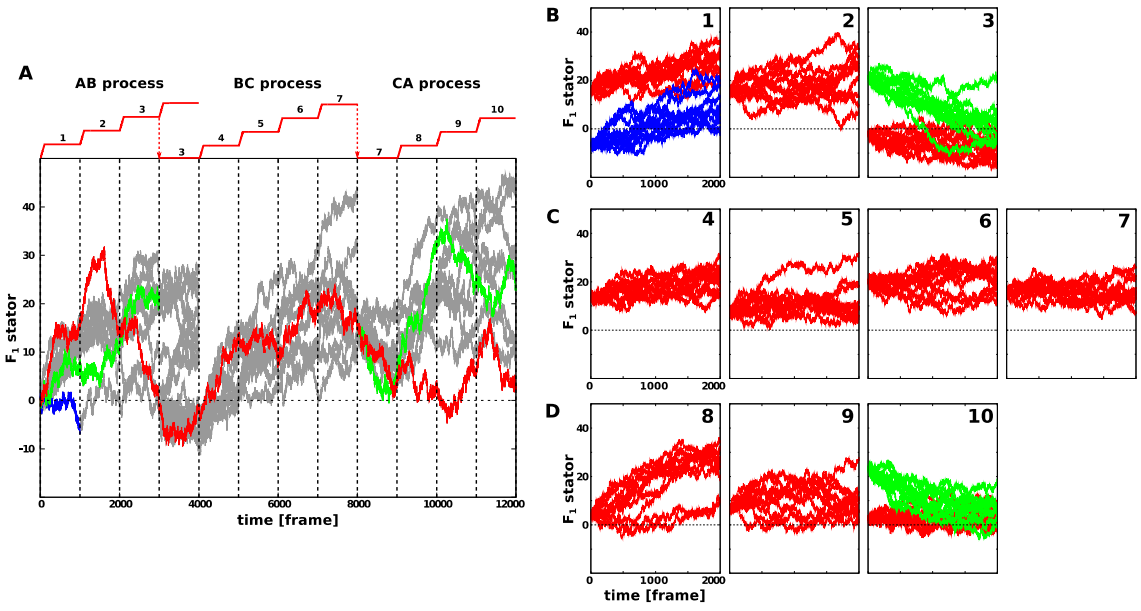

Fig. 4 Relaxation simulation with the c_{10}-ring rotation angle fixed at every n × 36º step.

a. Reference trajectories from which relaxation simulations were conducted. The F_1 stator rotation angle is depicted. Red: the representative one plotted in Figs. 2 and 3. Green in 0-3000th frame: one that was rotated markedly at the 3000th frame. Green in 8000-12000th frame: a case where the F_1 stator was largely rotated at the end. Blue: a case where the F_1 stator was least rotated. Gray: all the other trajectories. **b-d.** Each panel plots the time course of the F_1 stator angle in the relaxation simulation with c_{10}-ring fixed to the $n \times 36^\circ$ rotation angle. Each simulation started from the snapshot of the reference trajectory in **a** at the corresponding time. **b.** the c_{10}-ring rotation state n =1, 2, and 3 in the AB process. **c.** n =4, 5, 6, and 7 in the BC process. **d.** n =8, 9, and 10 in the CA process.

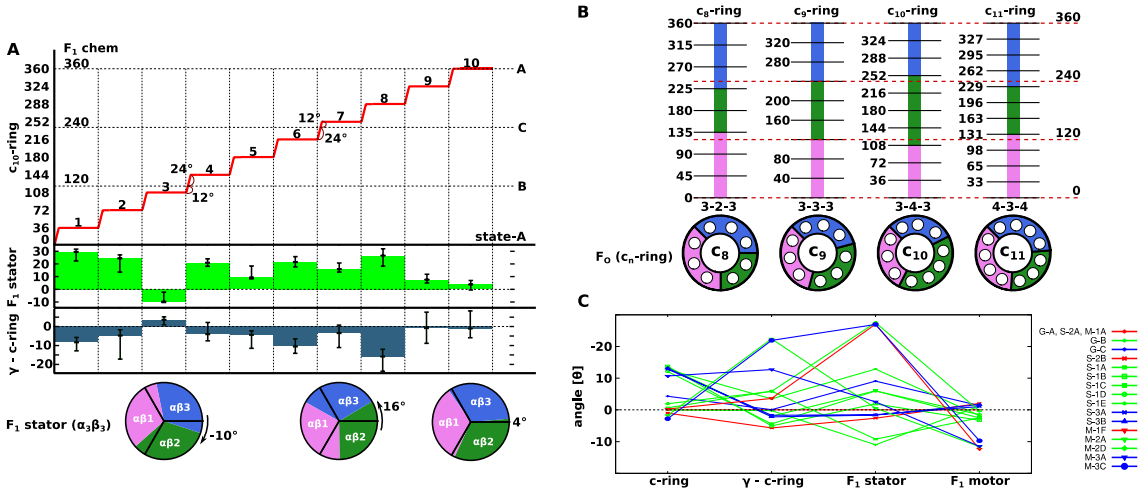

Fig. 5 The F_O-F_1 coupling and the symmetry mismatch in ATP synthesis process.

a. Summary of the symmetry mismatch and the elastic structure changes. The stepwise c_{10}-ring rotation (the red ladder), the F_1 motor rotation (the horizontal dashed line), the F_1 stator rotation via the distortion of the b-subunit (the green bar in the second panel), and the rotor distortion (the blue bar in the third panel) are depicted for every n × 36º c_{10}-ring rotation step. **b**. Predicted rotation pathways are described for systems with different number of c-subunits. **c**. Four elements of structure distortions found in cryo-EM studies. c-ring, the deviation of the c-ring rotation angle from its ideal angle. γ- c-ring, the rotary angle of the γ-subunit at its interaction site to αβ minus the c-ring rotation

564 angle. F_1 stator, the F_1 stator rotation angle relative to the F_O stator. F_1 motor, the rotation of the γ-

565 subunit relative to the F_1 stator $\alpha_3\beta_3$.

566

Table 1 Rotary angles in cryo-EM structures of three ATP synthases.

Guo	c_{10}-ring	n[1)]	$\gamma - c_{10}$-ring[2)]	F_1 stator[3)]	F_1 motor[4)]	m[5)]
6N2Y (state-A)	0	0/10	0	0	0	0/3
6N2Z (state-B)	108.0(-0.0)	3	-0.2	-11.0	118.8 (1.2)	1
6N30 (state-C)	247.7(4.3)	7	0.1	9.1	238.7 (1.3)	2
Sobti						
6WNQ (2A) A^{Guo}	0	0/10	0	0	0	0/3
6OQV (2B)	-1.0(-1.0)	0/10	-5.7	-2.6	-2.0 (2.0)	0/3
6OQR (1A) B^{Guo}	107.3 (0.7)	3	6.0	-9.2	122.5 (-2.5)	1
6OQS (1B)	130.3 (13.7)	4	-5.1	1.9	123.3 (-3.3)	1
6OQT (1C)	130.6 (13.4)	4	-2.0	6.0	122.5 (-2.5)	1
6OQU (1D)	131.9 (12.1)	4	-4.4	6.0	121.5 (-1.5)	1
6PQV (1E)	131.2 (12.8)	4	3.5	12.9	121.8 (-1.8)	1
6OQW (3A) C^{Guo}	239.1 (12.98)	7	-1.7	-1.5	238.9 (1.1)	2
6WNR(3B)	238.8 (13.2)	7	-2.2	-1.7	238.3 (1.7)	2
Murphy						
6RDH(1A) A^{Guo}	0	0/10	0	0	0	0/3
6RDW(1F)	35.7 (0.3)	1	3.6	27.1	12.3 (-12.3)	0/3
6RDZ(2A) B^{Guo}	109.8 (-1.8)	3	22.4	0.6	131.6 (-11.6)	1
6RE8(2D)	142.1 (1.9)	4	5.8	27.5	120.4 (-0.4)	1
6REB(3A) C^{Guo}	241.3 (10.7)	7	12.7	2.6	251.5 (-11.5)	2
6RES(3C)	254.8 (-2.8)	7	21.9	26.9	249.7 (-9.7)	2

The angle value is in degrees. The value in parentheses is the deviation from the ideal value from its symmetry.

[1)] The c_{10}-ring rotation step. [2)] The distortion of the rotor is defined by the difference between the angle of the upper part of the γ-subunit and the rotation angle of the c-ring. [3)] The rotation angle of the F_1 stator relative to the F_O stator. [4)] The difference between the angles of the F_1 stator and F_1 rotor. [5)] F_1 motor rotation step.